Infrared Physics & Technology 76 (2016) 710–721

Contents lists available at ScienceDirect

Infrared Physics & Technology

journal homepage: www.elsevier.com/locate/infrared

Regular article

An infrared image based methodology for breast lesions screening

K.C.C. Morais [a], J.V.C. Vargas [a,*], G.G. Reisemberger [b], F.N.P. Freitas [b], S.H. Oliari [b], M.L. Brioschi [c], M.H. Louveira [d], C. Spautz [d], F.G. Dias [d], P. Gasperin Jr. [d], V.M. Budel [d], R.A.G. Cordeiro [e], A.P.P. Schittini [e], C.D. Neto [c]

[a] Programa de Pós-Graduação em Engenharia e Ciência dos Materiais, Universidade Federal do Paraná, Curitiba, PR 81531-980, Brazil
[b] Departamento de Engenharia Mecânica, Universidade Federal do Paraná, Curitiba, PR 81531-980, Brazil
[c] Faculdade de Medicina da Universidade de São Paulo (FMUSP), Pós-Graduação em Termografia Médica, São Paulo, SP 01246-903, Brazil
[d] Hospital de Clínicas da Universidade Federal do Paraná, Centro da Mama, Curitiba 80060-900, Brazil
[e] Universidade Federal do Paraná, Centro de Atenção à Saúde – Casa III, Curitiba 81531-980, Brazil

HIGHLIGHTS

- We introduce a structured procedure for breast lesions screening.
- Infrared imaging temperature measurements are utilized.
- A normalized conjugate gradients methodology is tested.
- 101 individuals in control group and 47 breast cancer patients.
- 96% of the cases were detected.

ARTICLE INFO

Article history:
Received 8 August 2015
Accepted 28 April 2016
Available online 30 April 2016

Keywords:
Breast abnormalities
Infrared imaging
Conjugated gradients methodology

ABSTRACT

The objective of this paper is to evaluate the potential of utilizing a structured methodology for breast lesions screening, based on infrared imaging temperature measurements of a healthy control group to establish expected normality ranges, and of breast cancer patients, previously diagnosed through biopsies of the affected regions. An analysis of the systematic error of the infrared camera skin temperature measurements was conducted in several different regions of the body, by direct comparison to high precision thermistor temperature measurements, showing that infrared camera temperatures are consistently around 2 °C above the thermistor temperatures. Therefore, a method of conjugated gradients is proposed to eliminate the infrared camera direct temperature measurement imprecision, by calculating the temperature difference between two points to cancel out the error. The method takes into account the human body approximate bilateral symmetry, and compares measured dimensionless temperature difference values ($\Delta\bar{\theta}$) between two symmetric regions of the patient's breast, that takes into account the breast region, the surrounding ambient and the individual core temperatures, and doing so, the results interpretation for different individuals become simple and non subjective. The range of normal whole breast average dimensionless temperature differences for 101 healthy individuals was determined, and admitting that the breasts temperatures exhibit a unimodal normal distribution, the healthy normal range for each region was considered to be the dimensionless temperature difference plus/minus twice the standard deviation of the measurements, $\overline{\Delta\bar{\theta}} + 2\sigma_{\overline{\Delta\bar{\theta}}}$, in order to represent 95% of the population. Forty-seven patients with previously diagnosed breast cancer through biopsies were examined with the method, which was capable of detecting breast abnormalities in 45 cases (96%). Therefore, the conjugated gradients method was considered effective in breast lesions screening through infrared imaging in order to recommend a biopsy, even with the use of a low optical resolution camera (160 × 120 pixels) and a thermal resolution of 0.1 °C, whose results were compared to the results of a higher resolution camera (320 × 240 pixels). The main conclusion is that the results demonstrate that the method has potential for utilization as a noninvasive screening exam for individuals with breast complaints, indicating whether the patient should be submitted to a biopsy or not.

* Corresponding author.
E-mail address: jvargas@demec.ufpr.br (J.V.C. Vargas).

http://dx.doi.org/10.1016/j.infrared.2016.04.036
1350-4495/

Nomenclature

A_Ω	area of the affected region (m^2)
B_a	bias limit of quantity a
BI-RADS	Breast Imaging-Reporting and Data System
CASA III	UFPR Health Care Center
CEP	Brazilian Human Research Committee
CI	confidence interval
CT	computerized tomography
HC	Hospital of Clinics at UFPR
INCA	Brazilian National Cancer Institute
MLO	oblique midlateral position
MRI	magnetic resonance imaging
n	number of individuals in the sample
N_p	patient number
NPDEAS	Center for Sustainable Energy Research and Development
p	probability in a Student distribution
P_a	precision limit of quantity a
PET	positron emission tomography
R	resistance (Ω)
SPECT	photon emission computerized tomography
SQP	sequential quadratic programming
t	Student distribution test
T	temperature (°C)
U_a	uncertainty of quantity a
x, y	cartesian coordinates (m)
$\bar{x}$	sample mean
z	desired number of standard deviations

Greek symbols

α	body region
ΔT	temperature difference (°C)
$\Delta\bar{\theta}$	average dimensionless temperature difference of a skin region
$\overline{\Delta\bar{\theta}}$	the mean of all $\Delta\bar{\theta}$ in group ii (control)
ε	calculated error
θ	dimensionless temperature difference on a point
λ	normality range
μ	population mean
σ_a	standard deviation of quantity a
Ω	affected region domain, Fig. 1

Subscripts

b	body
c	infrared camera
FLIR	infrared camera FLIR E60
max	maximum value of a region in one individual
min	minimum value of a region in one individual
SAT	infrared camera SAT-S160
t	high precision thermistor
∞	ambient

Superscript

–	average value

1. Introduction

Most breast tumors are invasive, i.e., they could infiltrate in other tissues. They start in the breast lobules or ducts, but as the duct breaks, the breast surrounding tissues are invaded. The invasive breast cancer malignancy is strongly influenced by the sickness stage, i.e., the cancer extension or dissemination when it is diagnosed for the first time, thus early stage diagnosis becomes vital for a good prognosis [1].

The incidence of breast cancer new cases in the United States was 145.6/100,000 individuals, while in Brazil was 66.8/100,000 individuals in 2012. In the same year, the breast cancer mortality rate in the United States was 27.5/100,000 and 16.3/100,000 in Brazil, respectively [2]. The current breast cancer mortality rates remain high, most likely because the disease is still diagnosed in advanced stages. The Brazilian National Cancer Institute (INCA), and the Brazilian Ministry of Health estimated that 576,000 new cases of cancer would occur in 2014, from which breast cancer comprised 57,000 new cases, the most common among women of different listed types of cancer [3].

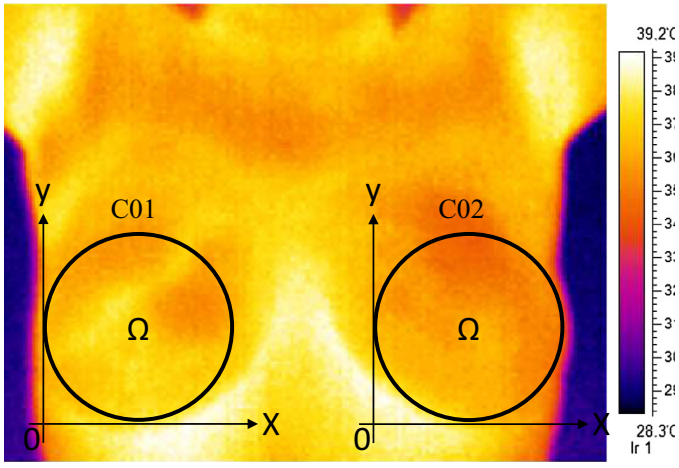

Fig. 1. Regions of interest.

Based on such facts, there is a need for the development of non-invasive methods to improve early diagnosis and screening of suspicious breast lesions [4–6]. One possible direction is the use of infrared imaging.

The human body skin temperature is a good health indicator although the temperature differences between a healthy and a sick individual are only marginal [7]. In the case of cancer, the cells are bigger than the normal cells, thus the cells need more energy, causing an increase in local irrigation and in skin temperature, i.e., there are more blood vessels to provide the necessary extra energy for them, that could be detected by the infrared camera [8,9]. Also, the ambient temperature, the individual metabolism and calibration parameters of the infrared camera are factors that affect the infrared imaging results [10].

Several non invasive diagnosis strategies for breast related diseases have been proposed in recent years, but no infrared imaging technique has achieved the status of possibly conducting patient screening before recommending a biopsy. Commonly used imaging modalities include mammography, ultrasonography, magnetic resonance imaging (MRI), scintimammography, single photon emission computerized tomography (SPECT) and positron emission tomography (PET) [11].

The mammography is considered the main breast cancer diagnosis method at the initial stage, capable of detecting small growths still non perceptible to the hand touch, and therefore favoring early treatment, effective, and non aggressive, with good aesthetic results, and few adverse events. The exam reveals small

and hidden malign lesions in asymptomatic women, i.e., at the early stage, allowing for a more favorable prognostic than the self exam [12–14]. However, there are indications that X-rays could potentially induce cancer, and it is well known that the mammography exam requires a tumor size of at least a few millimeters to be detected. It is also known that at such stage the tumor has already around a hundred million cells [15].

In spite of the value of the mammography in revealing breast malignancies, many of the radiologically identified lesions turn out benign in the histopathologic evaluation. According to American statistics around two thirds to four fifths of all performed biopsies are benign lesions [16,17]. Therefore, non invasive methods are needed to distinguish between benign and malign lesions.

The role of ultrasound in breast imaging has been largely limited to applications such as distinguishing between cystic versus solid masses, evaluation of palpable masses, and for needle core biopsy. In recent years, the number of indications has been greatly expanded and breast ultrasonography is now an essential modality in breast imaging. Independent clinical trials for women at high risk of hereditary breast cancer indicate increased sensitivity with breast MRI more than mammography, but with variable specificity [11].

Although promising, the MRI and Computerized Tomography (CT) images are considered very expensive for routine use. The MRI has not been found cost effective in young patients due to the identification of a large number of benign lesions in comparison to malign lesions. For soft tissues, the MRI is one of the main resources for medical diagnosis because internal anatomic details are clearly shown, and image quality is better than X-ray tomography [18,19]. Accordingly, the technological evolution of infrared camera design has increased the popularity of infrared imaging in medicine practice in recent years, since it is a non-invasive, low cost and a potentially large spectrum application technique [8].

In search of an infrared image analysis methodology for diagnosis of breast cancer, Bezerra [20] recommended the development of a standardized protocol for the acquisition of breast thermal images, including the design, construction and installation of a mechanical apparatus. Also, a methodology was presented to estimate thermal properties of the breast based on infrared images. However, the difficulty for the numerical computation of breast temperature profiles is caused by the uncertainty of the actual values of the thermophysical parameters of some tissues. The sequential quadratic programming (SQP) method was used to solve the inverse problem and estimate the thermal conductivity and breast tissue blood perfusion. Acharya [21] applied infrared imaging techniques for analysis of the eye ocular surface temperature of 67 healthy subjects. The absolute average temperature and standard deviation were determined to study the variability of the ocular surface showing different temperature ranges for different age groups with $p < 0.05$.

The bibliographic review shows that high resolution infrared imaging is still an emerging diagnosis and treatment monitoring tool in medicine, although its first reported medical use dates back to the mid 1950's [22,23]. However, it is a well established field in engineering. The main reason for that contrast is the lack of a non subjective protocol in medicine to associate skin temperature readings to physiological phenomena, since the exposed body surface is highly dependent on human metabolic conditions and surrounding environment. Also, differently from what occurs in engineering where high temperatures may be compared to significant lower ones, in the medical field normal or abnormal temperatures are slightly distinct. Therefore, methodologies to normalize temperature readings for any location and individual would be of great use in medicine. Additionally, the elimination of subjectivity in the interpretation of the breast skin temperature readings could eventually turn medical infrared imaging into a reliable technique for breast lesions screening.

1.1. Objective of the paper

The general objective of this work is to study the viability of utilizing infrared imaging as a noninvasive screening exam for suspicious breast lesions before recommending a biopsy. For that, a normalized conjugated gradients methodology is utilized, and tested with a group of 47 breast cancer patients previously diagnosed through biopsies.

2. Materials and methods

Between the months of August 2013 and February 2015, breast infrared images were taken from 47 female patients under breast cancer investigation that also took biopsies at the Tocoginecology Department in the Hospital of Clinics of Federal University of Parana, HC-UFPR, Curitiba, Parana, Brazil. Additionally, breast infrared images were taken from 101 female individuals with no complaints, that had no visible asymmetries between the right and left breasts, and mammographies or breast ultrasonographies with Breast Imaging-Reporting and Data System (BI-RADS) Assessment Category below 3 (probably benign).

Two infrared cameras were utilized in the study: (i) Sensor ThermaCAM T400 FLIR E60 (FLIR Systems Inc, North Billerica, Suécia), 320×240 pixels, electromagnetic wave spectral range between 7.5 and 13 μm, corresponding to the far infrared (FIR) range, with a reported ±1 °C temperature bias limit, 0.05 °C temperature resolution, and (ii) SAT-S160 (Guangzhou SAT Infrared Technology Co., Ltd., China), 160×120 pixels, electromagnetic wave spectral range between 7.5 and 14 μm, corresponding to the far infrared (FIR) range, with a reported ±2 °C temperature bias limit, 0.1 °C temperature resolution.

The study was conducted in six steps:

- The definition of two groups of study;
- The utilization of the normalized conjugated gradients methodology;
- The determination of the infrared camera systematic error;
- The comparison of infrared cameras with different image resolutions;
- The establishment of a normal range for the breasts' dimensionless temperature difference, and
- The application of the methodology to identify breasts' malignant growths through infrared imaging.

2.1. The definition of two groups of study

The following groups of study were defined:

i. Patients with malignant lesions, and
ii. Control: female individuals with no complaints.

Forty-seven patients with mammographies or breast ultrasonography with BI-RADS Assessment Category greater than or equal to 4 (suspicious abnormality) or equal to 0 (inconclusive), and diagnosed with breast cancer by a biopsy were selected to compose group i. For the control group, 101 female individuals with no complaints, and mammographies or breast ultrasonographies with BI-RADS Assessment Category less or equal to 3 (probably benign), and different from 0 (inconclusive) were selected to compose group ii. Therefore, the group should include healthy women that could statistically represent the entire female human population, considering all ages.

Aiming at reducing the influence of variables that are not related to the scope of the methodology, i.e., noninvasive early diagnosis of breast malignant growths, inclusion and exclusion criteria were established mainly for the control group, but three exclusion criteria are also necessary for group i. The selected criteria are listed as follows:

a. Inclusion criteria:
   1. Individuals without breast complaints;
   2. Individuals with normal mammography or ultrasonography, and
   3. Individuals with no visible localized temperature asymmetries in the infrared image.
b. Exclusion criteria:
   1. Patients that had undergone a mastectomy procedure, previous breast cancer surgery or treatment, loss of one or both nipples, or with acute breast inflammation, for both groups;
   2. Patients that have had breast implants, for both groups;
   3. Patients that used oral hormonal medication or were in hormonal therapy, and
   4. Patients that were going through a breast feeding period, for both groups.

The criterion of absence of visible localized temperature asymmetries in the infrared image was found indispensable, since innate vascular abnormalities may exist, even in young women, and without breast anomalies. The analysis requires the camera to be properly adjusted in order to identify clear asymmetries in the infrared image color distribution.

2.2. The utilization of the normalized conjugated gradients methodology

With the evolution of infrared camera technology, the medical interest on such noninvasive technique for possible disease early diagnosis has returned to grow due to low cost and potential for ample application. However, camera calibration parameters, ambient temperature, and the individual metabolism are factors that affect infrared imaging results. Therefore, it is commonly recognized that it is hard to determine accurately the difference in camera measurements between a healthy and a sick individual.

In order to cope with the problems listed in the previous paragraph, in this work, the recently proposed normalized conjugated gradients methodology [24] was utilized for evaluating patients with breasts' malignant growths. The method compares temperature measurements between two symmetric regions (e.g., right and left breasts).

2.2.1. Description

The methodology uses the dimensionless temperature proposed by Vargas et al. [10] to interpret the infrared camera temperature readings. The full description of the methodology is available in the work of Flores-Sahagun et al. [24], and only the conceptual equations are herein presented for clarity, as follows:

$$\theta = \frac{T - T_\infty}{T_b - T_\infty} \tag{1}$$

The emissivity of the human skin is approximately 0.98 ± 0.01 [25,26]. However, small variations in emissivity may result in considerable error (2–3 °C) in the value of the local surface temperature [27]. Therefore, in order to avoid systematic errors due to infrared camera calibration, two symmetric regions are defined (e.g., regions C01 and C02 in Fig. 1; regions C01 and C02, regions C03 and C04 in Fig. 2). The systematic calibration error of the camera (Bias limit, mostly due to the assignment of an inadequate patient skin surface emissivity value) is then cancelled out, and the only remaining error is the precision limit of the temperature measurement [28]. As a result, the dimensionless mean temperature difference between the two regions is analyzed, which is calculated as follows [24]:

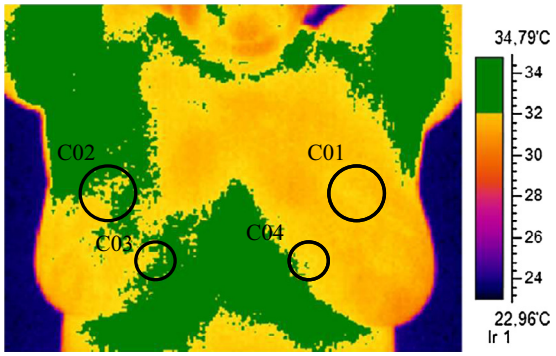

Fig. 2. Infrared image of breasts with the occurrence of two asymmetric regions (C01/C02 and C03/C04) that were marked with circles.

$$\Delta\bar{\theta} = |\bar{\theta}_1 - \bar{\theta}_2| \tag{2}$$

An individual breast region of analysis that includes the point of interest is defined, i.e., the affected region, as shown in Fig. 1, in which a circle or a polygonal line defines a domain (Ω) with respect to two cartesian axes x and y;

The mean dimensionless temperature for the entire region of interest is evaluated by [10,24]:

$$\bar{\theta} = \frac{1}{A_\Omega}\int\int_\Omega \theta(x,y)\mathrm{d}x\mathrm{d}y = \frac{\bar{T} - T_\infty}{T_b - T_\infty} \tag{3}$$

2.2.2. Sample size

The sample size for this study was estimated based on the following hypotheses: ❶ for breast temperatures of a female population that follows approximately a symmetric unimodal normal distribution; ❷ with a population standard deviation, σ; ❸ for samples greater than 30, $n > 30$, and ❹ for infinite populations. For that, according to probability and statistics theory, it is possible to estimate the sample size from a desired error, or the error from a given sample size through [29]:

$$n = \left(z\frac{\sigma}{\varepsilon}\right)^2; \quad \varepsilon = z\frac{\sigma}{\sqrt{n}} \tag{4}$$

where n is the number of individuals in the sample; z is the desired number of standard deviations such that the sample mean corresponds to the population mean within a desired confidence interval (CI); ε is the calculated error via $\varepsilon = \bar{x} - \mu$, in which $\bar{x}$ is the sample mean and μ the population mean, which is established in this study as a fraction of the population standard deviation, according to the investigation interest.

In this way, a desired error equal to 20% of the population standard deviation was established, i.e., $\varepsilon = 0.2\sigma$, and for CI = 95%, $z = 2$ [29]. Hence, the sample size calculated from Eq. (4) is $n = 100$. As a result, 101 healthy female individuals were selected for group ii, which also complied with the criteria listed in item 2.1.

After the infrared imaging measurements of groups i and ii, with 101 and 47 individuals, respectively, the test t of Student [29] was performed in order to verify the acceptance or not of the null hypothesis (groups have no significant differences). The p value was less than 5%, therefore the null hypothesis failed, and the two groups had significant differences indeed, with CI = 95%.

2.2.3. Infrared images reproducibility

An experiment was performed to evaluate the reproducibility of the infrared images, through the analysis of the temperature variation in time of several images of the same individual. For the experiment, the infrared images were taken from a 48-year old volunteer that had a normal mammography, BI-RADS 2 (Benign finding), and complied with the criteria listed in Section 2.1. The patient remained in anteroposterior position for a period of 30 min, so that 100 pictures were taken from the breasts and the eyes region.

One hundred consecutive images of the woman's breasts were taken, and the conjugated gradients method was applied. The possible variation in $\Delta\bar{\theta}$ calculated with Eq. (2) was analyzed, which included the possible variation in skin, ambient, and body temperature. The objective was to investigate if there would be a need to perform several measurements of the same individual or not. The standard deviation of the 100 images was calculated, and since it was less than 1% of the mean, it was found that there was no need to take more than one infrared image from each one of all tested individuals in this study.

2.2.4. Temperature measurements

The thermal images obtained from patients who comprised the control group were taken in the Center for Research and Development of Sustainable Energy (NPDEAS) or the Health Care Center (CASA III) at UFPR. All patients participating in this study signed the free and informed consent agreeing to the procedures for conducting the infrared imaging examination.

The infrared camera was placed on a fixed tripod horizontally 1 m away from the region of interest on the patient's breast in the standing posture, in order to ensure the same view factor and dimensions for the selected region of interest in all images. In this way, the camera lens was parallel to the region of interest surface. The patient was kept without clothes on the upper body, i.e., with naked breasts. Body temperatures (equivalent to the oral temperature) were taken with a digital Instant Thermometer (Geratherm, Germany) in the auditory canal. The average of three measurements taken with the same digital thermometer was used to estimate the ambient temperature near the patient in the test room. The windows and doors were always closed in order to keep the ambient wind free, with low humidity and thermal fluctuations.

Temperature measurements were also taken high precision thermistors of type YSI44004 (YSI Inc., USA), standard type Bead I, with a maximum diameter of 2.4 mm. They were utilized to estimate the infrared camera systematic error in this work.

2.2.5. Uncertainty analysis

In this work, the temperature measurements uncertainties were estimated according to standard criteria from the American Society of Mechanical Engineers, ASME [28]. The temperature measurements uncertainties are therefore obtained as follows:

$$U_T = \sqrt{P_T^2 + B_T^2}, \tag{5}$$

where B_T is the infrared camera bias limit, and P_T the precision limit, which is calculated as twice the standard deviation of all measurements performed for a particular case, $2\sigma_T$. Therefore, U_T is the temperature measurements uncertainty.

Based on Eq. (3), it is verified that:

$$U_{\Delta\bar{\theta}} \cong \frac{U_{\Delta\bar{T}}}{T_b - T_\infty} \cong \frac{P_{\Delta\bar{T}}}{T_b - T_\infty} = P_{\Delta\bar{\theta}} = 2\sigma_{\Delta\bar{\theta}} \tag{6}$$

where T_b and T_∞ are assumed approximately constant during the measurements, and $P_{\Delta\bar{T}} \gg B_{\Delta\bar{T}}$ according to the discussion presented before Eq. (2), in which it is shown that the Bias limit for $\Delta\bar{\theta}$ is practically cancelled out through the conjugated gradients methodology.

2.3. The determination of the infrared camera systematic error

An analysis to determine the infrared camera systematic error observed in the temperature measurements made with the camera was conducted. The objective was to demonstrate that temperature measurements made with the infrared camera on a surface show errors in the values obtained after the transformation of the surface radiation variation into temperature values. As it was discussed in the paragraph before Eq. (2), that transformation depends on the surface emissivity value, which is a parameter that has to be set in the camera, and that leads to an error in the final value of the measured temperature. Such phenomenon happens because the emissivity shows variations from one surface type to another, as for example the skins of two different individuals. This is one of the motivations for the utilization of the conjugated gradients methodology as discussed previously in the text.

In order to determine the camera systematic error, several skin regions were selected (hands, feet, breasts, arms), the temperature measurements were taken with high precision thermistors and with the infrared camera. After that, the difference between the two measurements was calculated.

The infrared images temperature measurements, T_c, and the thermistors ones, T_t, were compared as follows:

$$\Delta T = T_c - T_t \tag{7}$$

The thermistor temperature was taken by placing the sensor in direct contact with the skin surface, and sticking it to the skin with a thermally insulated tape in order to minimize thermal contact with the ambient.

2.4. The comparison of infrared cameras with different image resolutions

As discussed previously in the text, the infrared images were obtained with two cameras: SAT-S160 and FLIR E60. Both cameras have almost the same technical specifications, and have a detector that operates in the spectral range starting from the far infrared. However, there is a difference in image resolution. The higher the resolution the more details an image will display. The FLIR E60 camera features a resolution of 320×240 pixels, which is higher than the 160×120 pixels resolution offered by the SAT-S160 camera. Therefore, the question to be answered is: what is the effect of the different camera resolutions on the calculation of $\Delta\bar{\theta}$ according to Eq. (2) for the application of the conjugated gradients methodology?

In order to answer the question posed in the previous paragraph, symmetric regions were selected to perform a comparison of $\Delta\bar{\theta}$ measured with the two cameras: eyes, breasts, hands and feet (plantar and dorsal region) with a total of six images for each patient.

For taking the infrared images, a simple protocol was established in order to make sure the comparisons were accurate. All adornments, like rings and bracelets, were removed from the hands, the fingers were set apart in the same direction on a surface, then the infrared images were taken, first the back and then the palm of the hand, and the same methodology was followed for the feet. The regions of interest in the infrared images for calculating $\Delta\bar{\theta}$ were selected with circles of the same area, i.e., with the same diameter.

2.5. The establishment of a normal range for the breasts' dimensionless temperature difference

The normality range, i.e., the range of expected normal dimensionless temperature differences according to the conjugated gradients methodology, was determined assuming that the population follows a symmetric unimodal normal distribution. In this way, 95% of the measured dimensionless temperature differences are expected to fall within the mean value plus or minus twice the standard deviation of all measurements performed in group i (control group) [29].

The calculation of $\Delta\bar{\theta}$ resulted from the temperature measurements of infrared images of the right and left breasts that were marked with two equal circles as shown in Fig. 1, which visually presented thermal distributions approximately symmetric. Then, the standard deviation of the population sample that defined group ii (101 individuals) was calculated, and in order to represent 95% of the population, the normality range, λ, was given by:

$$\lambda = \overline{\Delta\bar{\theta}} \pm 2\sigma_{\overline{\Delta\bar{\theta}}} \quad (8)$$

in which $\overline{\Delta\bar{\theta}}$ is the mean of all $\Delta\bar{\theta}$ values in group ii, and $\sigma_{\overline{\Delta\bar{\theta}}}$ is the sample standard deviation of the measurements.

2.6. The application of the methodology to identify breasts' malignant growths through infrared imaging

The conjugated gradients methodology that was described in Section 2.2 was applied to a group of women without complaints, and previously considered in normal conditions either by ultrasonography or mammography (group ii – control), and to a group of patients previously diagnosed with breast malignant growths by biopsies (group i). During the infrared imaging acquisition, it was realized that small size localized asymmetries existed in some patients, i.e., as compared to the total breast size. In these cases, the calculation of $\Delta\bar{\theta}$ with Eq. (2) based upon the full breast led to a value within the normality range, λ, i.e., to the occurrence of some false negative results. Therefore, there was a need for a more specific method with potential to detect all malignant growth cases.

As a result, in order to perform the individuals screening via infrared imaging, it is suggested that the conjugate gradients methodology should be coupled to the identification of localized breast temperature asymmetries, and the following steps are proposed:

(i) Search for the occurrence of visible localized asymmetries between the two breasts based on the infrared image color distribution. A nonsubjective procedure is explained with the help of Fig. 3, which shows a sequence of three images of the same patient. From Fig. 3a–c, the image color scale (refinement) is changed gradually until an asymmetric temperature point or region becomes visible in the comparison between the two breasts. In Fig. 3a no asymmetries are seen, then refining the color scale, in Fig. 3b a circle is drawn around the left breast highlighting the occurrence of asymmetric regions, which become more evident with further color refinement in Fig. 3c. In this way, it is possible to locate one or more points (regions) where the temperature is different in one breast from the other, and perform the analysis with the conjugated gradient method only in the selected regions that are smaller than the full breast. For example, Fig. 2 allows for the comparison of regions C01 and C02, and regions C03 and C04;

(ii) After the procedure of step (i), if color asymmetries are not clearly identifiable, perform the analysis drawing circles around the full breasts as it is shown in Fig. 1, and calculate the corresponding value of $\Delta\bar{\theta}$;

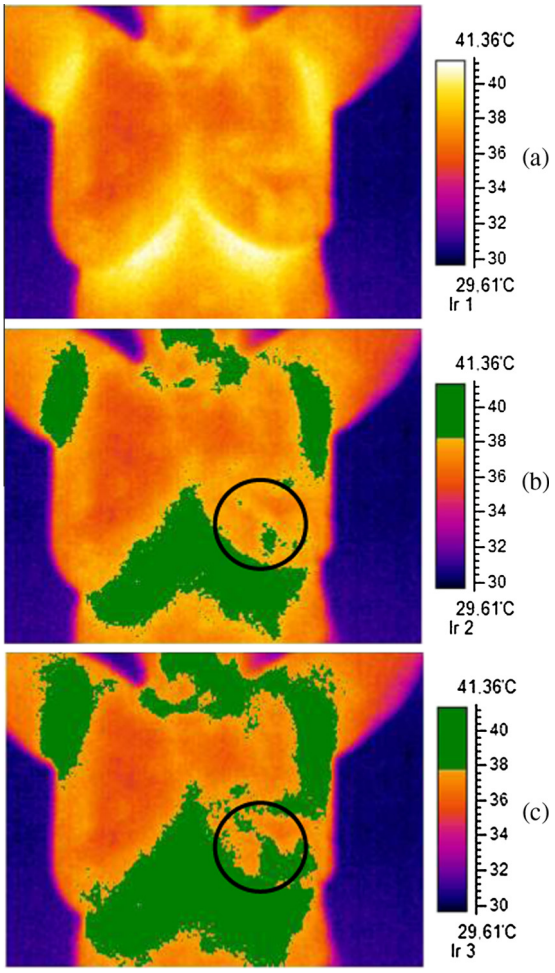

Fig. 3. The gradual image color scale refinement from (a) no asymmetries, (b) initial color refinement showing the occurrence of asymmetric regions, and (c) further color refinement showing more evident asymmetries. (For interpretation of the references to color in this figure legend, the reader is referred to the web version of this article.)

(iii) When visible asymmetries are found according to step (i), as it is shown in Fig. 2, for example, draw circles around the selected localized asymmetries, and calculate the corresponding values of $\Delta\bar{\theta}$. It is important to point out that more than one region could be selected, as many as the analyst deems necessary, and

(iv) In all situations, check if $\Delta\bar{\theta}$ of the analyzed regions is outside the normality range, λ, defined by Eq. (8). In such case, it is recommended that the patient should be submitted to the traditional procedures of ultrasonography, mammography and biopsy. On the other hand, if $\Delta\bar{\theta}$ of the analyzed regions is within the normality range, the infrared imaging exam does not indicate the need to proceed to additional exams.

3. Results and discussion

Based on the methodology presented in the previous section, with groups i (47 patients diagnosed with breasts malignant growths via biopsies) and group ii (control – 101 individuals with lesion free breasts), results were obtained, and are herein presented and discussed. Sequentially, the infrared camera systematic error is assessed, infrared images of two cameras with different resolutions are compared, the normal range for the breasts' dimen-

sionless temperature is depicted, and finally the conjugated gradients methodology is utilized to identify breasts' malignant growths.

3.1. The determination of the infrared camera systematic error

According to the methodology presented in Section 2.3, the infrared camera systematic error was determined. Table 1 shows the temperature measured data collected from different regions of the human body, α (hands: 1-left; 2-right, feet: 3-left; 4-right, breasts: 5-left; 6-right and arms: 7-left; 8-right) taken once, using a high precision thermistor and the infrared camera, and the temperature difference between them, according to Eq. (7).

In order to produce the results of Table 2, a series of temperature measurements were performed in triplicate with a high precision thermistor, and with the infrared camera from the different parts of the human body. Then, the temperature differences mean between thermistor and infrared camera was calculated for the investigated human body regions, $\Delta\bar{T}$, and the standard deviation $\sigma_{\Delta\bar{T}}$. The results show that there is indeed a systematic error in the temperatures measured with the infrared camera utilized in this study (SAT-S160) between 2.2 and 2.4 °C, which is probably due to the device calibration and the adopted skin emissivity value, as discussed previously in the text. The same results are shown graphically in Fig. 4. The analysis of Table 2 and Fig. 4 demonstrates the existence of the infrared camera systematic error in any skin surface temperature direct measurement, therefore any interpretation of temperature measurements would be biased by such error. The conjugated gradients methodology is one possible way to correct the infrared camera systematic error, according to the explanation presented in Section 2.2.

3.2. The comparison of infrared cameras with different image resolutions

Four volunteers from group ii (control – 101 individuals with lesion free breasts) participated of the analysis presented in this section. Table 3 shows a compilation of all measurements. Five regions of the human body were selected to perform the comparison, i.e., breast, eyes, back and palm of the hand, forefoot and sole of the foot. The conjugated gradients methodology was applied to calculate $\Delta\bar{\theta}$ for each region for both cameras. The comparison was made in terms of the mean temperature difference for each region, which is shown in the last column of Table 3. Based on the differences observed between the data obtained with the two cameras utilized in this study, a mean value for $|\Delta\bar{\theta}_{SAT} - \Delta\bar{\theta}_{FLIR}|$ was calculated as 0.002, with a standard deviation of 0.003. The analysis of the results of Table 3 show that the observed differences are at least 1 order of magnitude (10 times) smaller than the measured $\Delta\bar{\theta}$. Hence, it is reasonable to state that with the conjugate gradients methodology, it is indifferent to use one camera or the other, in spite of the much better resolution of the camera FLIR E60.

Table 1
Infrared camera and thermistor temperature difference of the measurements in four regions of the body.

α	T_t (°C)	T_c (°C)	ΔT(°C)
1. Left hand	31.6353	33.9	2.2647
2. Right hand	31.6353	33.9	2.2647
3. Left foot	29.5383	31.8	2.2617
4. Right foot	29.1425	31.4	2.2575
5. Left breast	32.2306	34.5	2.2694
6. Right breast	32.0825	34.3	2.2175
7. Left arm	33.3134	35.6	2.2866
8. Right arm	34.1210	36.4	2.2790

Table 2
The calculation of the infrared camera systematic error through temperature measurements in four regions of the body.

α	$\Delta\bar{T} - 2\sigma_{\Delta\bar{T}}$ (°C)	$\Delta\bar{T} + 2\sigma_{\Delta\bar{T}}$ (°C)	$\Delta\bar{T}$ (°C)	$P_{\Delta\bar{T}} = 2\sigma_{\Delta\bar{T}}$ (°C)
1. Left hand	2.2	2.4	2.3	0.1
2. Right hand	2.0	2.7	2.3	0.4
3. Left foot	2.0	2.6	2.3	0.3
4. Right foot	2.2	2.6	2.4	0.2
5. Left breast	2.2	2.6	2.4	0.2
6. Right breast	2.1	2.7	2.4	0.3
7. Left arm	1.8	2.7	2.2	0.5
8. Right arm	2.2	2.6	2.4	0.2

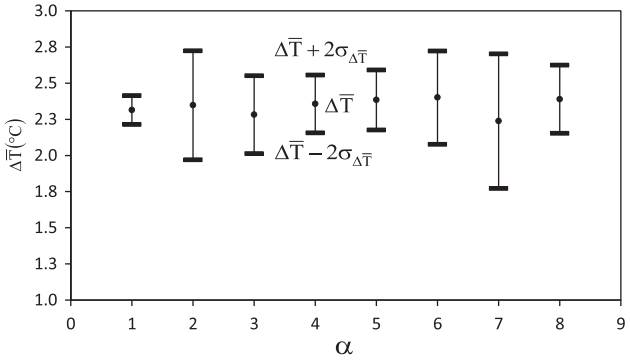

Fig. 4. The infrared camera systematic error in direct temperature measurements.

Table 3
The comparison of the measured $\Delta\bar{\theta}$ by two infrared cameras with different image resolutions in six regions of the body in 4 different individuals.

Individual	Body regions	$\Delta\bar{\theta}$		$\lvert\Delta\bar{\theta}_{SAT} - \Delta\bar{\theta}_{FLIR}\rvert$
		SAT S160	FLIR E60	
1	Breast	0.0394	0.0391	0.0003
	Eyes	0.0243	0.0279	0.0036
	Back of the hand	0.0117	0.0112	0.0006
	Palm of the hand	0.0142	0.0168	0.0025
	Forefoot	0.0444	0.0447	0.0003
	Sole of the foot	0.0562	0.0559	0.0003
2	Breast	0.0241	0.0247	0.0006
	Eyes	0.0010	0.0000	0.0010
	Back of the hand	0.0452	0.0432	0.0020
	Palm of the hand	0.0060	0.0062	0.0001
	Forefoot	0.0312	0.0309	0.0003
	Sole of the foot	0.0814	0.0802	0.0012
3	Breast	0.0008	0.0000	0.0008
	Eyes	0.0176	0.0185	0.0009
	Back of the hand	0.0168	0.0185	0.0018
	Palm of the hand	0.0168	0.0185	0.0018
	Forefoot	0.0176	0.0185	0.0009
	Sole of the foot	0.0243	0.0247	0.0004
4	Breast	0.0121	0.0124	0.0004
	Eyes	0.0060	0.0062	0.0002
	Back of the hand	0.0586	0.0559	0.0027
	Palm of the hand	0.0870	0.0745	0.0125
	Forefoot	0.0121	0.0031	0.0090
	Sole of the foot	0.0009	0.0000	0.0009

Specifically for the breasts, the smallest difference was 0.0003 whereas the largest one was 0.0008, i.e., significantly smaller than the difference observed in other regions, which is probably due to the fact that the breasts are located in highly irrigated region of the body, therefore minimizing the benefits that could result from the image acquisition with a high resolution camera.

Based on the data of Table 3, the Student t distribution was utilized to verify if there was significant difference between the SAT-S160 and FLIR E60 measurements. The result was $p = 0.91$, therefore it is possible to conclude that there are no significant differences between the measurements taken with the two cameras, since $p > 0.05$. This conclusion is important, in the sense that the higher the camera resolution the more expensive the camera will be. Therefore, the results demonstrate that the conjugate gradients methodology has the potential to allow for reliable data acquisition and data interpretation even with low cost infrared cameras.

3.3. The establishment of a normal range for the breasts' dimensionless temperature difference

According to the criteria and methodology established in Sections 2.1,2.2, and 2.5, 101 women were evaluated, and considered free of breast lesions to form group ii (control). Based on the $\Delta\bar{\theta}$ values found for group ii (control), it was possible to establish a normality range according to Eq. (8), $\lambda = \overline{\Delta\bar{\theta}} \pm 2\sigma_{\Delta\bar{\theta}} = 0.0130 \pm 0.0170$. Fig. 5 shows graphically the distribution of the measured $\Delta\bar{\theta}$ values. The dotted line represents the mean of the obtained values, $\overline{\Delta\bar{\theta}}$, and the solid line shows the upper bound of the normality range, i.e., $\lambda = 0.0130 + 0.0170$. Hence, it is reasonable to state that any individual that exhibits a measured $\Delta\bar{\theta}$ value within that range is expected not to have breast abnormalities with CI = 95%, otherwise she/he should be directed to a biopsy exam.

3.4. The application of the methodology to identify breasts' malignant growths through infrared imaging

In order to experimentally validate the normality range found in Section 3.3, in this section infrared images were taken from 47 patients diagnosed by histopathology after biopsies (group i). The conjugated gradients methodology was applied and the obtained $\Delta\bar{\theta}$ values were compared with the normality range shown in Fig. 5. Table 4 shows the patient number, code, the breast in which the lesion was found, the BI-RADS assessment category/lesion location in the breast, and finally the type of carcinoma found through the histopathology after the biopsy.

Fig. 6a shows the results of the method considering only the full breast, i.e., drawing circles around the full breasts, and calculating $\Delta\bar{\theta}$ according to Eq. (2). It is verified the occurrence of 25 false negatives, i.e., patients with malignant lesions diagnosed by histopathology that fell within the normality range. The physical reason for that to happen, as discussed previously in the text is that for a small lesion compared to the size of the full breast, due to a non-significant increase in local vascularization, the corresponding local increase in temperature is not enough to affect the full breast average temperature. This observation inspired the development of a refined conjugated gradients methodology presented in Section 2.6, which was tested with the same group of patients.

The measured $\Delta\bar{\theta}$ values for the 47 (forty-seven) patients in group i are drawn in Fig. 6b. The application of the conjugated gradients methodology followed the steps described in Section 2.6, i.e., identifying properly localized temperature asymmetries in the breasts and drawing a circle only in the region around them for conducting the analysis. As a result, only 2 (two) patients fell within the normality range, characterizing false negatives.

The results show that the conjugate gradients methodology coupled to a localized breast temperature asymmetries technique still presented false negatives (2 cases in 47 patients). A possible explanation for that is that such false negatives corresponded to very small size tumors (diameter < 1 mm), therefore with a morphology that did not imply in significant increase in the local vascularization.

At this point, it is important to note that the consecrated breast screening methods such as ultrasonography and mammography also display false negatives in similar rates. Therefore, it is expected that infrared imaging applied with the conjugated gradients method could be a useful screening tool in the early detection of breast abnormalities.

After the determination of the results, the Student t test was utilized to compare the two groups. The obtained result was $p = 0.0$, i.e., $p < 0.05(5\%)$, thus there is significant difference between the two groups. The analysis was conducted considering the results of group i obtained with the conjugated gradients method coupled to the localized temperature asymmetries technique.

Next, in order to illustrate the application of the methodology, two examples are discussed in detail. Two patients are analyzed both by infrared imaging, ultrasonography, and histopathology.

Patient code 249, 59 years old, had a palpable nodule in the left breast associated to nipple bleeding. The ultrasonography showed the existence of a hypoechoic solid nodule, with irregular edges, oblique to the skin with internal vascularization, located in the upper outer quadrant (QSL), next to the anterior armpit line, measuring 14 × 11 × 16 mm, and classified the lesion as BI-RADS IVc, i.e., a high grade suspicious abnormality. The infrared image of the patient is shown in Fig. 7, which depicts an evident temperature distribution asymmetry between the right and left breasts. The left breast displays higher temperatures than the right breast. Probably due to the nipple blood discharge, the breast vascularization is increased, and the temperature is elevated not only in the

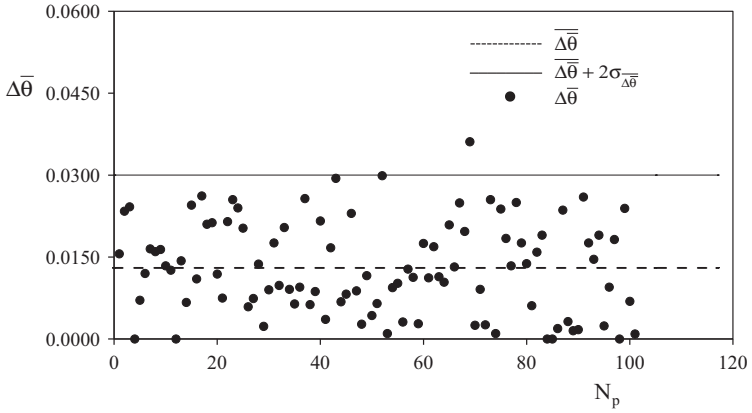

Fig. 5. The measured $\Delta\bar{\theta}$ for the 101 individuals of group ii (control), the mean of the entire group, $\overline{\Delta\bar{\theta}}$, and the normality range upper bound, $\overline{\Delta\bar{\theta}} + 2\sigma_{\overline{\Delta\bar{\theta}}}$ (solid line).

Table 4
The list of the tested 47 patients (group i) with the tumor breast location, BI-RADS assessment via mammography or ultrasonography, lesion location, and histopathology.

N_p	Patient code	Breast (R:Right/ L:Left)	BI-RADS assessment category/lesion location in the breast	Type of carcinoma (Histopathology)
1	206	R	BI-RADS IV (Mammography)	Ductal carcinoma in situ
2	207	R	BI-RADS 0 (Mammography)	Invasive ductal carcinoma
3	210	L	BI-RADS IV (Ultrasonography)	Invasive ductal carcinoma
4	214	R	BI-RADS IV (Mammography)/QSM	Invasive ductal carcinoma
5	215	R	(Ultrasonography)/UQlat	Invasive ductal carcinoma
6	216	L	BI-RADS IV (Mammography)/QSL	Invasive ductal carcinoma
7	217	R	BI-RADS V (Mammography)	Ductal carcinoma in situ
8	221	R	BI-RADS IVB (Ultrasonography)/QSL	Invasive ductal carcinoma
9	226	R	BI-RADS V (Mammography)/QSL	Invasive ductal carcinoma
10	236	L	BI-RADS IV (Mammography)/QSM	Invasive ductal carcinoma
11	239	L	BI-RADS IV (Mammography)/UQsup	Invasive ductal carcinoma
12	240	L	BI-RADS IV (Mammography)/RRA	Invasive ductal carcinoma
13	241	L	BI-RADS IV (Mammography)/QSL	Invasive ductal carcinoma
14	242	R	BI-RADS IV (Mammography)/QSL	Invasive ductal carcinoma
15	245	R	BI-RADS IVA (Ultrasonography)/QSL	Invasive ductal carcinoma
16	247	R	BI-RADS IVc (Ultrasonography)/QIM	Invasive ductal carcinoma
17	249	L	BI-RADS IVc (Ultrasonography)/QSL	Invasive ductal carcinoma
18	257	R	BI-RADS IV (Mammography)/UQlat	Invasive ductal carcinoma
19	261	R/L	BI-RADS 0 (Mammography)/Right: QSM. and Left: RRA	Invasive ductal carcinoma
20	269	L	BI-RADS IV (Mammography)/RRA	Invasive ductal carcinoma
21	270	L	BI-RADS IVc (Mammography)	Invasive ductal carcinoma
22	274	L	BI-RADS IVc (Mammography)	Ductal carcinoma in situ
23	275	L	BI-RADS V (Mammography)	Invasive ductal carcinoma
24	279	L	BI-RADS IV (Ultrasonography)/QSL	Invasive ductal carcinoma
25	281	R	BI-RADS V (Ultrasonography and Mammography)/UQsup	Invasive ductal carcinoma and ductal carcinoma in situ
26	283	R	BI-RADS V (Ultrasonography and Mammography)/QSL	Invasive ductal carcinoma andinvasive lobular carcinoma
27	291	R	BI-RADS IV (Ultrasonography)/UQinf and PA	Invasive lobular carcinoma
28	295	L	BI-RADS V (Ultrasonography)/UQlat	Invasive ductal carcinoma
29	298	L	BI-RADS II (Mammography)/Recent nipple retraction in the left breast and axillary lymph node palpable	Invasive lobular carcinoma
30	300	R	BI-RADS V (Mammography)/two nodules: UQsup and QSM	Invasive ductal carcinoma
31	301	L	BI-RADS IV (Mammography)/QSL	Invasive ductal carcinoma
32	303	R	(Ultrasonography)/QIL	Invasive ductal carcinoma and invasive lobular carcinoma
33	307	L	BI-RADS IVb (Ultrasonography)/QSL – nodule in the left breast with axillary lymph node	Invasive ductal carcinoma
34	311	R	BI-RADS V (Mammography)/QSL	Invasive ductal carcinoma
35	312	L	BI-RADS IV (Mammography)/QSM	Invasive lobular carcinoma
36	313	R	BI-RADS IV (Ultrasonography)/QIM	Invasive ductal carcinoma
37	314	L	BI-RADS IV (Ultrasonography)/QSL	Invasive ductal carcinoma
38	315	R	BI-RADS IVc (Mammography e Ultrasonography)/QIM	Invasive lobular carcinoma
39	316	L	BI-RADS IVa (Ultrasonography)	Ductal carcinoma in situ
40	320	R	BI-RADS V (Mammography)/QSL and PA	Invasive ductal carcinoma
41	323	L	BI-RADS IV (Mammography)/QSL	Invasive ductal carcinoma
42	325	R	BI-RADS V (Mammography)/QIM	Invasive ductal carcinoma
43	330	R	BI-RADS IV (Mammography)/UQsup	Invasive ductal carcinoma
44	335	L	BI-RADS IV (Mammography)/UQsup and RRA	Invasive ductal carcinoma
45	336	R	BI-RADS IV (Mammography)/QSL and PA	Invasive ductal carcinoma
46	339	L	BI-RADS III (Ultrasonography)/UQsup and PA	Invasive ductal carcinoma
47	344	R	BI-RADS III (Mammography)/UQlat	Invasive ductal carcinoma

QSL – upper outer quadrant; QIL – lower outer quadrant; QSM – upper inner quadrant; QIM – lower inner quadrant; UQlat – union of the lateral quadrants; UQsup – union of the upper quadrants; UQmed – union of the medial quadrants; UQinf – union of the lower quadrants; RRA – retroareolar; PA – axillary tail.

nodule region, but also in the entire breast. Histopathology after the biopsy diagnosed an invasive ductal carcinoma.

In the application of the conjugated gradient methodology drawing circles around the full breasts, $\Delta\bar{\theta} = 0.1239$, whereas the analysis coupled with the localized breast temperature asymmetries technique, i.e., selecting only the upper outer quadrant (QSL) according to the circles drawn in Fig. 7, $\Delta\bar{\theta} = 0.1504$, with both results being much higher than the upper bound of the normality range found with group ii (control). In this case, the infrared imaging exam was effective for an initial patient screening to indicate abnormality, which in turn recommended further investigation by the conventional screening methods, i.e., mammography and ultrasonography.

After the biopsy, for patient 257, 69 years old, histopathology diagnosed the existence of an invasive ductal carcinoma in the right breast. The ultrasonography detected microcalcifications in the union of the medial quadrants, UQmed, and a nodule in the union of the lateral quadrants, UQlat (<10 mm), both in the right breast, classified as BI-RADS IV. Fig. 8a shows the infrared image of the breasts anterior region, and Fig. 8b shows the mammographic image of the oblique midlateral position (MLO). By comparing Fig. 8a and b, it is verified that the infrared image indicates clearly a distinct elevated temperature region in the right breast corresponding exactly to the affected region detected by the mammography. However, for a concrete assessment, an infrared imaging non-subjective methodology is required.

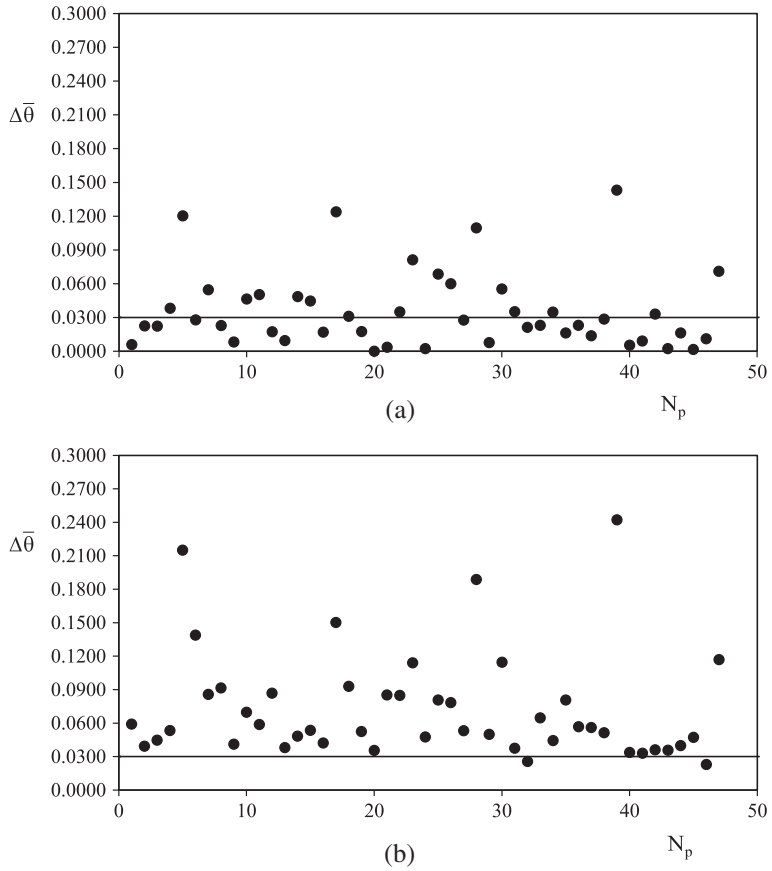

Fig. 6. The measured $\Delta\bar{\theta}$ for the 47 patients previously diagnosed by histopathology with breast carcinoma, i.e., group i, (a) calculated based on the full breast image, and (b) with the localized temperature asymmetries technique, together with the normality range upper bound, $\overline{\Delta\theta} + 2\sigma_{\overline{\Delta\theta}}$ (solid line).

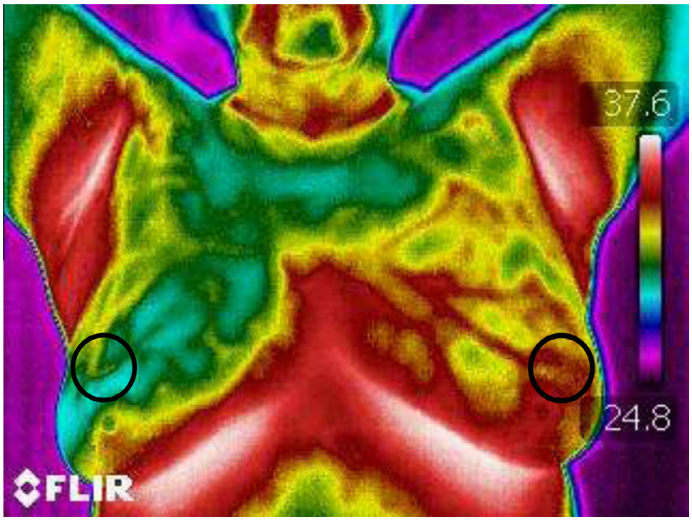

Fig. 7. Breasts infrared image of patient 249 with the identification of one localized temperature asymmetry.

The application of the conjugated gradients methodology drawing a circle around the full breasts obtained $\Delta\bar{\theta} = 0.031$, indicating that the value is practically on top of the upper bound of the normality range, so that the interpretation could be inconclusive, which is not correct, since mammography classifies the image as BI-RADS IV. However, the analysis coupled with the localized breast temperature asymmetries technique, i.e., selecting only the union of the lateral quadrants (UQlat) according to the circles drawn in Fig. 8a, found $\Delta\bar{\theta} = 0.093$, which is approximately three times the value of the upper bound of the normality range, i.e., clearly indicating an abnormality, which is correct.

Finally, it is important to point out that studies indicate that 80–90% of the identified breast carcinomas are of the type invasive ductal carcinoma [1,30,31]. The data shown in Table 4, that were

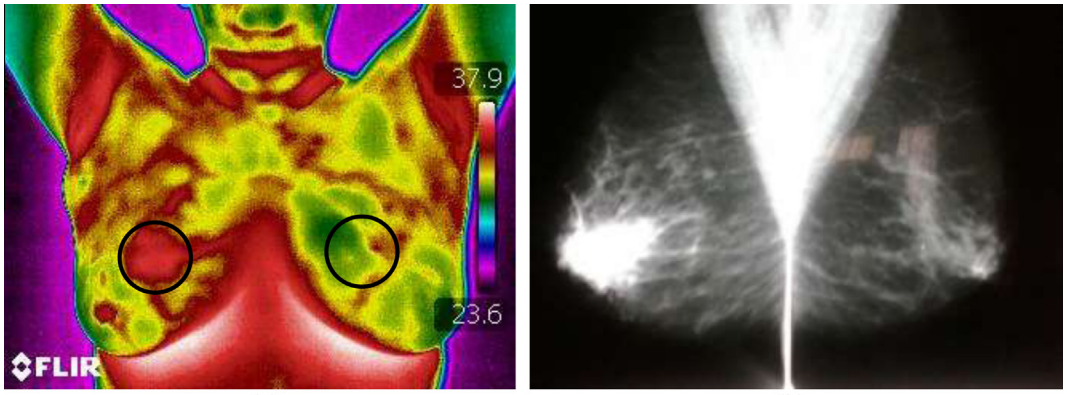

Fig. 8. (a) Breast infrared image of patient 257 with one high asymmetry in the union of the lateral quadrants, UQlat, and (b) mammographic image indicating the existence of a nodule.

obtained via histopathology of the 47 patients of group i, are in agreement with that information, since 85% of the studied patients presented that carcinoma type.

4. Conclusions

This study proposed and investigated the utilization of a normalized conjugated gradients method coupled to a localized temperature asymmetries technique for infrared imaging analysis. For that, the methodology was theoretically presented and applied to a set of patients that were previously diagnosed with breast carcinoma through biopsies followed by histopathology.

The key conclusions of this study are:

(1) The normalized conjugated gradients method is simple and was capable to differentiate normal from lesioned tissue, identifying breast carcinomas through the comparison of the measured patient's $\Delta\bar{\theta}$ of asymmetric temperatures breast regions with an expected breasts normality range $\overline{\Delta\bar{\theta}} + 2\sigma_{\overline{\Delta\bar{\theta}}}$, which was also determined through the application of the method to 101 individuals with lesion free breasts in a control group;
(2) The utilization of a dimensionless temperature, θ, compensates the temperature readings with respect to variations in the individual's metabolism and ambient temperature at the particular location of the exam, so that the expected normality ranges are general, i.e., independent of body and local ambient temperature;
(3) The application of a normalized conjugated gradients method coupled to a localized temperature asymmetries technique was effective to detect breast abnormalities, i.e., identifying 96% of the 47 studied breast carcinoma cases, whereas the normalized conjugated gradients method applied to the full breast detected only 53% of the 47 studied breast carcinoma cases, and
(4) The conjugated gradients method was efficient to identify breast lesions (which were associated to breast carcinoma through mammography, ultrasonography, together with biopsies followed by histopathology) even with the use of a camera of low optical resolution (160×120 pixels) and thermal resolution of 0.1 °C.

Possible follow up studies are recommended: (i) infrared imaging and the conjugated gradients methodology should be further investigated in order to be possibly used for the definition of a safe breast tumor excision margin, so that recurrence might be avoided; (ii) the normalized infrared imaging conjugated gradients methodology should also be further investigated to be possibly used for treatment follow up after breast tumor excision, periodically checking the patient (say every 6 months) for new tumor signs still non-detectable by other methods, and (iii) associate an image processing software to identify temperature asymmetric areas in order to avoid the dependence on a trained professional for the visual detection of the affected areas in the infrared image.

Ethical approval

The research project that developed this study was approved by ruling No. 339,545 of 23rd July 2013, from the Research Ethics Committee in Human Beings of the Hospital of Clinics at Federal University of Parana, Curitiba, Brazil, HC-UFPR.

Conflicts of interest

We declare that we have no conflict of interests.

Acknowledgements

The authors acknowledge with gratitude the support of the Brazilian National Council of Scientific and Technological Development, CNPq, via project 567997/2008-1, and the cooperation of the Hospital of Clinics at Federal University of Parana, Curitiba, Brazil (HC-UFPR), and the UFPR Health Care Center (CASA III).

References

[1] J.M. Edwards, S.M. Herzberg, J.W. Shook, T.K.N. Beirne, D.A. Schomas, Breast conservation therapy utilizing partial breast brachytherapy for early-stage cancer of the breast: a retrospective review from the Saint Luke's Cancer Institute, Am. J. Clin. Oncol.-Cancer Clin. Trials 38 (2) (2015) 174–178.
[2] L.A. Torre, F. Bray, R.L. Siegel, J. Ferlay, J. Lortet-Tieulent, A. Jemal, Global cancer statistics, 2012, CA-A Cancer J. Clin. 65 (2) (2015) 87–108.
[3] José Alencar Gomes da Silva National Cancer Institute, Estimate/2014 – cancer incidence in Brazil, Vigilance and Prevention General Coordination, Ministry of Health, 2014. (in Portuguese) ISBN 978-85-7318-236-1.
[4] S.A. Feig, Decreased breast cancer mortality through mammographic screening: results of clinical trials, Radiology 167 (1988) 659–665.
[5] J.R. Keyserlingk, P.D. Ahlgren, E. Yu, N. Belliveau, Infrared imaging of breast: initial reappraisal using high-resolution digital technology in 100 successive cases of stage I and II breast cancer, The Breast J. 4 (1998) 241–251.
[6] G.C. Wishart, M. Campisi, M. Boswell, D. Chapman, V. Schackleton, S. Iddles, A. Hallett, P.D. Britton, The accuracy of digital infrared imaging for breast cancer detection in women underdoing breast biopsy, J. Cancer Surg. 36 (2010) 535–540.
[7] C. Villaseñor-Mora, F.J. Sanchez-Marin, M.E. Garay-Sevilla, Contrast enhancement of mid and far infrared images of subcutaneous veins, Infrared Phys. Technol. 51 (2008) 221–228.

[8] A.C. Guyton, J.E. Hall, Medical Physiology Treatment, tenth ed., Mcgraw Hill Interamericana, Mexico, 2001 (in Spanish).
[9] C. Quek, W. Irawan, E.Y.K. Ng, A novel brain inspired neural cognitive approach to SARS thermal image analysis, Expert Syst. Appl. 37 (2010) 3040–3054.
[10] J.V.C. Vargas, M.L. Brioschi, F.G. Dias, M.B. Parolin, F.A. Mulinari-Brenner, J.C. Ordonez, D. Colman, Normalized methodology for medical infrared imaging, Infrared Phys. Technol. 52 (2009) 42–47.
[11] M. Herranz, A. Ruibal, Optical imaging in breast cancer diagnosis: the next evolution, J. Oncol. 2012 (2012) 1–10, http://dx.doi.org/10.1155/2012/863747.
[12] M.L. Sclowitz, A.M.B. Manezes, D.P. Gigante, S. Tessro, Conduts in the secondary prevention of breast cancer and associated factors, Publ. Health J. 39 (2005) 340–349 (in Portuguese).
[13] G.C. Wishart, M. Campisi, M. Boswell, D. Chapman, V. Shackleton, S. Iddles, A. Hallett, P.D. Britton, The accuracy of digital infrared imaging for breast cancer detection in women undergoing breast biopsy, Eur. J. Surg. Oncol. 36 (2010) 535–540.
[14] I.K. Maitra, S.K. Bandyopadhyay, Digital imaging in mammography towards detection and analysis of human breast cancer, Comput. Aided Soft Comput. Tech. Imaging Biomed. Appl. 1 (2010) 29–34.
[15] H. Hondermarck, Breast cancer – when proteomics challenges biological complexity, Mol. Cell. Proteomics 2 (2003) 281–291.
[16] L. Liberman, Clinical management issues in percutaneous core breast biopsy, Radiol. Clin. North Am. 38 (2000) 791–807.
[17] Y.R. Parisky, A. Sardi, R. Hamm, K. Hughes, L. Esserman, S. Rust, K. Callahan, Efficacy of computerized infrared imaging analysis to evaluate mammographically suspicious lesions, Am. J. Roentgenol. 180 (1) (2003) 263–269.
[18] I.J. Sanches, Thermographic images superposition and magnetic resonance: a new modality of tridimensional image, PhD Dissertation – Technology Sector, Federal Technology University of Parana, Curitiba, Brazil, 2009, 168 pages. (in Portuguese).
[19] B.R. Alvares, M. Michell, The utilization of magnetic resonance in the investigation of breast cancer, Braz. Radiol. 9 (2003) 373–378 (in Portuguese).
[20] M. Zavisek, Quantitative thermography in breast cancer detection – a survey of current research. Doctoral Degree Programme (2), Dept. of Biomedical Engineering, FEEC, BUT, Czech Republic, 2004.
[21] U.R. Acharya, Analysis of normal human eye with different age groups using infrared images, J. Med. Syst. 33 (2009) 207–213.
[22] R.N. Lawson, Implications of surface temperatures in the diagnosis of breast cancer, Can. Med. Assoc. J. 75 (1956) 309–315.
[23] J.D. Wallace, C.M. Cade, Clinical Thermography, CRC, Cleveland, OH, 1975.
[24] J.H. Flores-Sahagun, J.V.C. Vargas, F.A. Mulinari-Brenner, Analysis and diagnosis of basal cell carcinoma (BCC) via infrared imaging, Infrared Phys. Technol. 54 (2011) 367–378.
[25] J. Steketee, Spectral emissivity of skin and pericardium, Phys. Med. Biol. 18 (5) (1973) 686–694.
[26] B.F. Jones, A reappraisal of the use of infrared thermal mag analysis in medicine, IEEE Trans. Med. Imaging 17 (1998) 1019–1027.
[27] A. Bejan, Heat Transfer, Wiley, New York (1993) (Chapter 10).
[28] J.H. Kim, T.W. Simon, R. Viskanta, Journal of heat transfer policy on reporting uncertainties in experimental measurements and results [Editorial], J. Heat Transfer 115 (1993) 5–6.
[29] S. Lipschutz, M.L. Lipson, Theory and Problems of Probability, second ed., McGraw-Hill, New York, 2000.
[30] M. De Brot, F.A. Soares, M.M.A. Stiepcich, V.S. Cúrcio, H. Gobbi, Basal-like breast carcinomas: clinicopathologic and evolutive profile, Braz. Med. Assoc. J. 55 (2009) 529–534.
[31] H.J. Burstein, K. Polyak, J.S. Wong, S.C. Lester, C.M. Kaelin, Ductal carcinoma *in situ* of the breast, The New Engl. J. Med. 350 (2004) 1430–1441.